

# Investigation of Rocket Effect in Bright-Rimmed Clouds using *Gaia* EDR3

Piyali Saha,<sup>1,2,3\*</sup> Maheswar G.,<sup>2</sup> D. K. Ojha,<sup>4</sup> Tapas Baug,<sup>1</sup> and Sharma Neha<sup>5</sup>

<sup>1</sup>Satyendra Nath Bose National Centre for Basic Sciences, Salt Lake, Kolkata 700 106, India

<sup>2</sup>Indian Institute of Astrophysics (IIA), Sarjapur Road, Koramangala, Bangalore 560034, India

<sup>3</sup>Pt. Ravishankar Shukla University, Amanaka G.E. Road, Raipur, Chhattisgarh 492010, India

<sup>4</sup>Tata Institute of Fundamental Research (TIFR), Homi Bhabha Road, Mumbai 400005, India

<sup>5</sup>Aryabhatta Research Institute of Observational SciencES (ARIES), Manora Peak, Nainital 263002, India

arXiv:2207.04661v1 [astro-ph.SR] 11 Jul 2022

Accepted XXX. Received YYY; in original form ZZZ

## ABSTRACT

Bright-rimmed clouds (BRCs) are excellent laboratories to explore the radiation-driven implosion mode of star formation because they show evidence of triggered star formation. In our previous study, BRC 18 has been found to accelerate away from the direction of the ionizing HII region because of the well known “Rocket Effect”. Based on the assumption that both BRC 18 and the candidate young stellar objects (YSOs) are kinematically coupled and using the latest *Gaia* EDR3 measurements, we found that the relative proper motions of the candidate YSOs exhibit a tendency of moving away from the ionizing source. Using BRC 18 as a prototype, we made our further analysis for 21 more BRCs, a majority of which showed a similar trend. For most of the BRCs, the median angle of the relative proper motion of the candidate YSOs is similar to the angle of on-sky direction from the ionizing source to the central *IRAS* source of the BRC. Based on Pearson’s and Spearman’s correlation coefficients, we found a strong correlation between these two angles, which is further supported by the Kolmogorov-Smirnov (K–S) test on them. The strong correlation between these two angles supports the “Rocket Effect” in the BRCs on the plane-of-sky.

**Key words:** Stars: distances, pre-main-sequence, Proper motions, ISM: clouds

## 1 INTRODUCTION

The origination and evolution of massive stars can immensely affect the immediate surroundings where they form. The strong stellar winds or some supernova explosions may compress the nearby molecular clouds and thus trigger a subsequent formation of stars that otherwise may not have initiated. This is typically known as positive stellar feedback. In a converse scenario, the effect may be too intense that results in hindering further star formation activity by dispersing the pre-existing cloud material, which can be considered as negative stellar feedback. Thus stellar feedback has significant aftermaths in terms of cloud energetics, multiple stellar population, regulation of star formation rates, star formation efficiency, and so on (Zinnecker & Yorke 2007).

The strong ultraviolet radiation emitting from the massive stars, or expansion of HII regions, develops high-pressure waves by the ionizing heating into the surrounding pre-existing dense clumps. This enhanced pressure may trigger the birth of new proto-stellar cores or compress the pre-existing ones to eventually lead to formation of a new generation of stars. This mechanism of star formation triggered by radiation from neighbouring massive stars is known as radiation-driven implosion (RDI; Bertoldi 1989; Bertoldi &

McKee 1990). The consequent clouds are known as bright-rimmed clouds (BRCs; Sugitani et al. 1991; Sugitani & Ogura 1994), having their illuminated rim facing towards the ionizing star(s) and often tied up with an elongated structure along the opposite direction. They are isolated molecular clouds and often found to be located at the boundaries of evolved HII regions. Sugitani et al. (1991) and Sugitani & Ogura (1994) listed a total of 89 BRCs based on their association with the Infrared Astronomical Satellite (*IRAS*) sources. Observational evidence of star formation, e.g., *IRAS* point sources, H $\alpha$  emitting stars, infrared (IR) excess sources, Herbig-Haro objects, etc., were reported in those BRCs (e.g., Table 1 of Elmegreen 1998). Also, signposts of spatial distribution along with gradient in evolutionary stages of young stellar objects (YSOs) are detected along the axes of the BRCs, which is typically known as “small-scale sequential star formation” (e.g., Sugitani et al. 1995; Ogura et al. 2007; Choudhury et al. 2010). Thus, BRCs are considered to be the markers of positive stellar feedback in the formation of YSOs.

Several analytical studies were carried out to understand the evolution of clouds during the RDI mode (e.g., Oort & Spitzer 1955; Kahn 1969). The process starts when an ionization front preceded by a shock front travels across the dense globule, causing it to collapse and resulting in formation of a highly dense core, which eventually could trigger the star formation. The time at which the star formation begins and the

\* E-mail: s.piyal16@gmail.com (PS)

fraction of cloud material gets transformed into stars is typically  $\sim 10^5$  yrs (Saha et al. 2022, hereafter, Paper I). At the surface of ionization front, because of the enhanced pressure the ionized cloud material starts photo-evaporating towards the ionizing source and as a back reaction of the expelled ionized gas, the residual cloud escalates away from the direction of ionizing HII region, which is typically known as the ‘‘Rocket Effect’’ (hereafter, RE; Oort 1954). The YSOs formed by consequence of the RDI should share the kinematics similar to the accelerating cloud. Thus, the YSOs would accelerate radially away from the nearby massive star/s, which is/are responsible for ionizing the cloud and triggering the star formation in it (Dale et al. 2015).

To investigate the RE on the BRCs, we first examined the proper motion (PM) of candidate YSOs associated with BRC 18 in Paper I. BRC 18 resides at the eastern periphery of the  $\lambda$  Ori HII region. The strong ionizing photons coming from the earliest type star of the Collinder 69 cluster,  $\lambda$  Ori (O8III; Conti & Leep 1974), is considered to be responsible for the ongoing RDI mechanism in BRC 18 (Sugitani et al. 1991). Using the latest *Gaia* Early Data Release 3 (EDR3) astrometric measurements, we found that the majority of the candidate YSOs located towards BRC 18 share similar PM values and are lying at similar distances suggesting that they are all formed together and currently moving as a group. We then subtracted the median PM of the  $\lambda$  Ori HII region from the observed PMs of the candidate YSOs vectorially. This results in the true internal projected motions of these candidate YSOs. A similar approach was followed in other recent studies also, for example, Sicilia-Aguilar et al. (2019) and Arun et al. (2021). Fig. 1 shows a cartoon diagram of a system consisting of a BRC and one ionizing source (also see Paper I), where we depict the angles used in our analysis.  $\theta_{ip}$  and  $\theta_{pm}$  represent the angle of ionizing photons and the angle of the internal projected motion of YSOs, respectively. The  $\theta_{pm}$  is estimated by the median angle made by the relative PM or internal projected motion of the candidate YSOs, starting from celestial north and increasing eastward. We estimate the  $\theta_{ip}$  as the angle made by the line joining the ionizing source and the central *IRAS* source residing in each BRC (Paper I). The  $\theta_{ip}$  values are also measured following the same convention as it was done for  $\theta_{pm}$ . As discussed in Paper I, in an ideal RE scenario,  $\theta_{ip}$  is expected to be similar to  $\theta_{pm}$ , i.e.,  $|\theta_{ip} - \theta_{pm}| \approx 0^\circ$ , on the sky plane.

Both BRC 18 and Collinder 69 cluster, of which  $\lambda$  Ori is a part, reside at a similar distance ( $\sim 400$  pc; Paper I) indicating that both are lying almost on the sky plane. In BRC 18, we found  $|\theta_{ip} - \theta_{pm}| = 1^\circ \pm 14^\circ$ , which is very close to  $0^\circ$ , supporting the RE. Motivated by this finding we investigated the RE in additional 21 BRCs having a considerable number of candidate YSOs with reliable counterparts in the *Gaia* EDR3 archive. This paper is structured in the following manner. The archival data and data from literature are explained in section 2. A relevant discussion on the results is presented in section 3. Finally, we summarize and conclude our work in section 4.

## 2 ARCHIVAL DATA AND DATA FROM LITERATURE

Based on various methods, for example, Two Micron All Sky Survey (2MASS), *Spitzer*, *WISE* archival data and results from near- and mid-IR photometric observations (e.g.,

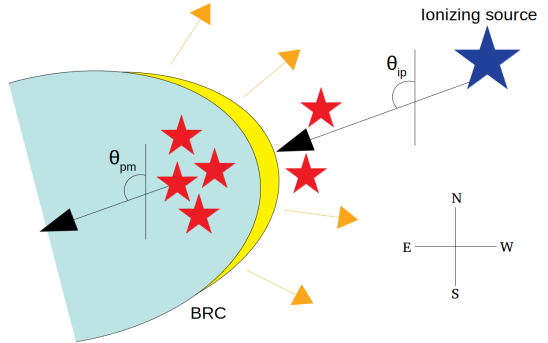


**Figure 1.** An illustration of a system consisting of a BRC (blue cloud with a thick yellow colored rim) and an ionizing source (blue star) (not to scale). The YSOs distributed towards the BRC are presented using red star symbols. The direction of photo-evaporation flow of the cloud material is shown using yellow colored arrows. The black colored arrow making an angle  $\theta_{ip}$  with respect to the north and directing away from the ionizing star, is the direction of ionizing photons. Another black colored arrow making an angle  $\theta_{pm}$  with respect to the same and directing away from the YSOs, presents the angle of their relative proper motion.

Hayashi et al. 2012; Panwar et al. 2014; Sharma et al. 2016), slitless spectroscopy (Ogura et al. 2002; Ikeda et al. 2008; Hosoya et al. 2020), optical BVI<sub>c</sub> photometry (e.g. Chauhan et al. 2009), optical spectroscopy (e.g. Choudhury et al. 2010; Kounkel et al. 2018), X-ray imaging (Getman et al. 2012), astrometry from *Gaia* data release 2 (DR2) (Kounkel et al. 2018; Zari et al. 2018), method of maximum likelihood (Getman et al. 2018), presence of the candidate YSOs in the BRCs has been reported. We collected information of all candidate YSOs available in these references for our study.

*Gaia* EDR3 (Gaia Collaboration et al. 2020) presents precisely measured astrometric parameters of more than one billion objects, brighter than  $G \sim 21$ . We acquired distances ( $d$ ) and PMs in right ascension ( $\mu_{\alpha*}$ ) and declination ( $\mu_\delta$ ) from Bailer-Jones et al. (2021) and the *Gaia* EDR3 archive (Gaia Collaboration et al. 2020), respectively, for our sources using a cross-match radius of  $1''$ . Sources having their ratios,  $d/\Delta d$ ,  $\mu_{\alpha*}/\Delta\mu_{\alpha*}$ , and  $\mu_\delta/\Delta\mu_\delta$  all are  $\geq 3$ , are considered for this study, where,  $\Delta d$ ,  $\Delta\mu_{\alpha*}$ , and  $\Delta\mu_\delta$  are the measurement uncertainties in  $d$ ,  $\mu_{\alpha*}$ , and  $\mu_\delta$ , respectively. In an unresolved multiple stellar system, the presence of an orbiting companion around a source introduces a wobble at the point of maximum flux. Thus, the barycenter of the stellar system shifts away from its photocenter. This, in turn, results in a poorer goodness-of-fit statistics, and comes up with a higher renormalized unit weight error (RUWE), which is considered as a reliable indicator of the existence of a nearby associate (e.g., Belokurov et al. 2020; Stassun & Torres 2021; Kervella et al. 2022). We included only those sources for which the RUWE  $\leq 1.4$  (Lindegren 2018). The selection criteria are also mentioned in Paper I.

## 3 RESULTS AND DISCUSSIONS

### 3.1 Selection of the BRCs

The methodology adopted here to affirm the coupling between young sources with their parental clouds is similar to

our previous studies (Saha et al. 2020, 2021, 2022). Based on the literature, out of 89 BRCs, candidate YSOs have been identified towards 52 of them using various methods till date (as described in section 2). Among the 52 BRCs, we selected 29 of them, which are associated with at least 4 candidate YSOs satisfying our selection criteria. The median absolute deviation (MAD) was used to compute the statistical dispersion in  $d$ ,  $\mu_{\alpha*}$ , and  $\mu_{\delta}$ . Only those candidate YSOs, which are lying within  $5 \times \text{MAD}$  with respect to the median values of the  $d$ ,  $\mu_{\alpha*}$ , and  $\mu_{\delta}$ , are selected as the members of each of their respective BRCs. The adoption of  $5 \times \text{MAD}$  was made because the majority of the candidate YSOs in the BRCs are distributed within this boundary. We recomputed the median and the MAD of  $d$ ,  $\mu_{\alpha*}$ , and  $\mu_{\delta}$  of the selected candidate YSOs to estimate the final astrometric results of the BRCs (also see Paper I).

Of the 29 BRCs, we first excluded BRCs 15, 24, and 30, where the candidate YSOs are distributed far from the cloud-ionizing star vicinities. Also, we excluded BRC 51 due to its high MAD in  $\mu_{\delta}$  ( $-2.187 \pm 6.657$  mas yr $^{-1}$ , obtained from *Gaia* EDR3 measurements of the candidate YSOs) from further study. Also, ionizing stars of this BRC ( $\zeta$  Pup and  $\gamma^2$  Vel; Thompson et al. 2004) do not have astrometric measurements in *Gaia* EDR3. Additionally, we set a numerical limit  $z = (d - d_*) / (\Delta d + \Delta d_*)$  for the consistency of distance between the BRC (or the candidate YSOs residing in the BRC) and the respective ionizing sources, where,  $d_*$  and  $\Delta d_*$  are the distance for the ionizing source and its corresponding uncertainty, respectively. In our study, we select only those BRCs, for which  $z \leq 1$ . Thus, BRCs 34, 68, and 76 were eliminated. Therefore, out of 29 BRCs, seven were excluded from our further analysis. In Tables 1 and 2 (available as supplementary material), we present the details of candidate YSOs in the BRCs along with the  $\theta_{pm}$  and  $\theta_{ip}$  found in the analysis. The strategies followed to obtain the  $\theta_{pm}$  of the candidate YSOs in the remaining 22 BRCs are discussed below:

**BRC 2:** The massive source responsible for ionization of BRC 2 is BD+66 1675, which does not fulfill our selection criteria. We used the median PM obtained from the members of the HII region Sh2-171, which are associated with BD+66 1675 (Getman et al. 2018; Panwar et al. 2018), as the reference to obtain the  $\theta_{pm}$ .

**BRCs 5 and 7:** Three early type sources, BD+60 502, BD+60 504, and BD+60 507, are considered to influence BRCs 5 and 7 (Ishida 1970; Morgan et al. 2004). BD+60 504, and BD+60 507 both have good astrometric measurements and reside at  $2122^{121}_{-81}$  and  $1960^{65}_{-68}$  pc, respectively. We used the PMs of BD+60 504 as the reference as its  $d$  is more consistent with the BRCs.

**BRCs 17 and 18:** BRCs 17 and 18 reside at the  $\lambda$  Ori HII region and considered to be ionized by  $\lambda$ -Ori (Sugitani et al. 1991). The methodology adopted to find the relative PM of the candidate YSOs in these BRCs is described in Paper I.

**BRC 25:** The massive source considered to ionize BRC 25 is HD 47839, which has a higher RUWE making its astrometric measurements unreliable. Therefore, we obtained the reference PM values of NGC 2264 from Buckner et al. (2020) to estimate the  $\theta_{pm}$ .

**BRCs 36 to 39:** BRCs 36-39, located in the HII region IC 1396, are considered to be ionized by the central ionizing source HD 206267 (Sugitani et al. 1991), which fails our selection criteria. Therefore, we used median PM values of the

cluster members of IC 1396 provided in the literature (Contreras et al. 2002; Sicilia-Aguilar et al. 2005; Mercer et al. 2009; Sicilia-Aguilar et al. 2019) as the reference to compute the  $\theta_{pm}$  of the candidate YSOs in the BRCs.

**BRC 55:** For BRC 55, in the HII region RCW 27, the massive source responsible for ionizing BRC 55 is HD 73882, which has RUWE = 2.068. Therefore, we obtained the astrometric parameters of the members of RCW 27 (Prisinzano et al. 2018) from *Gaia* EDR3 and used the median PM of the cluster members as the reference PM to estimate  $\theta_{pm}$ .

**BRC 64:** The star responsible for ionizing BRC 64 is LSS2231, located at  $3145^{400}_{-437}$  pc, while BRC 64 resides at  $2968 \pm 225$  pc. Thus the lower limit of  $d$  of LSS2231 lies within the distance range of BRC 64. Though the RUWE of LSS2231 is 1.819, this is to note that it satisfies all of our other selection criteria. Due to lack of information of any other members of the HII region BBW 347 where BRC 64 resides, we used the PM values of LSS2231 to estimate the  $\theta_{pm}$ .

**BRC 65:** There are three early type sources considered to ionize BRC 65, which are, HD 101131, HD 101205, and HD 101436 (Thompson et al. 2004), located in the HII region RCW 62. As only HD 101205 satisfies our selection criteria, we used its PM values as the reference to compute the  $\theta_{pm}$ .

**BRC 79:** BRC 79 is found to be located in the HII region RCW 108. Two massive sources are found to be responsible for the ionization of this region, HD 150136 (O5III) and HD 150135 (O6.5V) (Thompson et al. 2004). As  $d$  of HD 150136 ( $1428^{93}_{-96}$  pc) is more consistent than HD 150135 ( $1242^{37}_{-39}$  pc) with the same for BRC 79, and the spectral type of HD 150136 is earlier than the later, we considered the PM of HD 150136 as the reference PM.

**BRC 82:** Three early type sources, HD 152233 (O6III), HD 326286 (B0), and HD 152245 (B0Ib) are considered to be responsible for the ionization of BRC 82 (Yamaguchi et al. 1999; Thompson et al. 2004). The earliest type ionizing source, HD 152233, is a member of the cluster NGC 6231. As there is a high possibility of the influence of other massive stars of NGC 6231, we obtained median PM of the cluster members from Kuhn et al. (2017) and considered those as reference PM.

The rest BRCs, i.e., 11, 26, 27, 31, 54, 75, and 89 are associated with HII regions having reliable astrometric measurements of the ionizing sources in the *Gaia* EDR3 catalogue. Therefore, the PMs of these ionizing sources were used as the reference PMs in order to investigate the RE taking place in the respective BRCs.

### 3.2 Internal projected motion of the candidate YSOs in the BRCs

Our study finally focuses on 22 BRCs (including BRC 18), which consist of a considerable number of candidate YSOs with reliable astrometric measurements in *Gaia* EDR3. Mostly the YSOs are embedded deep in the natal cloud, so the optical emission from many of them are highly obscured by the circumstellar and interstellar dust resulting in unreliable or no detection in *Gaia* EDR3. In Fig. 2 (a) we present the distribution of  $\theta_{ip}$  versus  $\theta_{pm}$  of 22 BRCs. BRCs 54 and 89 show distinctively higher  $|\theta_{ip} - \theta_{pm}|$  compared to other BRCs. We marked them using open circles. Other 20 BRCs are shown using filled grey circles. We made two cases A and B, which indicate inclusion and exclusion of both BRCs 54 and 89, respectively. The solid black line

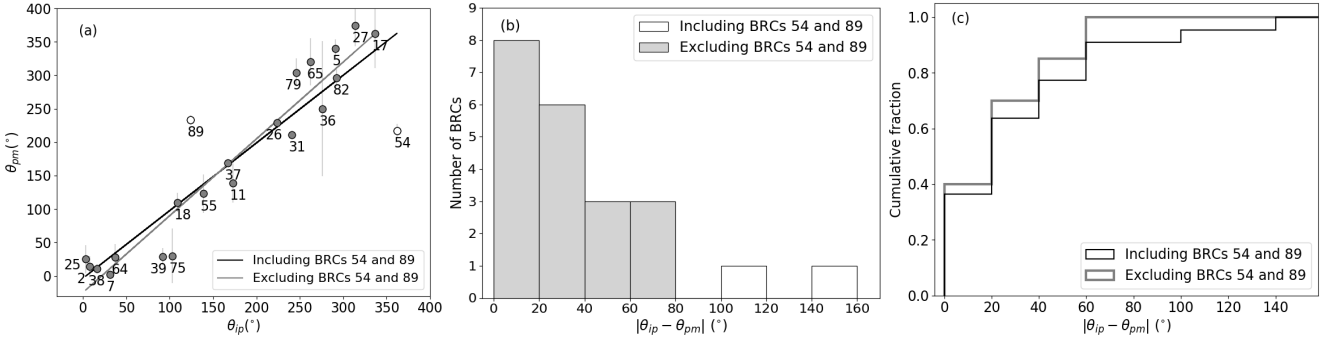


**Figure 2.** (a) Plot of  $\theta_{ip}$  versus  $\theta_{pm}$ . The solid black line shows the best-fitted line for 22 BRCs (case A). The solid grey line shows the best-fitted line for 20 BRCs, excluding BRCs 54 and 89 (case B). (b) Histogram of  $|\theta_{ip} - \theta_{pm}|$  for the BRCs with bin size  $\sim 20^\circ$ . (c) Cumulative histogram of the distribution of  $|\theta_{ip} - \theta_{pm}|$  for the BRCs with bin size  $\sim 20^\circ$ .

shows the best-fitted line for case A. The slope of this line is estimated as  $1.011 \pm 0.103$ . We again show the best-fitted line in case B using solid grey line, of which the slope is estimated as  $1.148 \pm 0.071$ . Error in  $\theta_{pm}$  is estimated using the error propagation method. The error in  $\theta_{ip}$  is negligible because the positional errors of the sources are in milli arcsecond order. To obtain the correlation between  $\theta_{ip}$  and  $\theta_{pm}$ , we computed the Pearson's correlation coefficient. For case A, the value is found to be 0.909 with pnull  $4.641 \times 10^{-9}$ . The Spearman's correlation coefficient is estimated as 0.899, with pnull as  $1.247 \times 10^{-8}$ . We also performed Kolmogorov-Smirnov (K-S) test on these angles. The computed statistic is 0.182, and the pvalue is 0.821. For case B, the Pearson's and Spearman's correlation coefficients for 20 BRCs are estimated as 0.967 and 0.964 with pnull  $3.444 \times 10^{-12}$  and  $8.654 \times 10^{-12}$ , respectively. The K-S test provides statistic of 0.200, and the pvalue is 0.771 for the 20 BRCs. All these statistical analyses indicate a strong correlation between  $\theta_{ip}$  and  $\theta_{pm}$ . The distribution of  $|\theta_{ip} - \theta_{pm}|$  as a form of histogram with binsize  $20^\circ$  is shown in Fig. 2 (b), using white- and grey-colored bins, for cases A and B, respectively. A maximum in the lowest of  $|\theta_{ip} - \theta_{pm}|$  and a decrease in the number of BRCs with higher  $|\theta_{ip} - \theta_{pm}|$  is clearly noticeable. In Fig. 2 (c), we show the cumulative histogram of  $|\theta_{ip} - \theta_{pm}|$ , using white- and grey-colored bins, for cases A and B, respectively. It is apparent from both Figs. 2 (b) and (c), that almost  $\sim 80\%$  of the BRCs show  $|\theta_{ip} - \theta_{pm}| \leq 60^\circ$ .

This is to note that because of the lack of information of the radial velocities of the sources, in Paper I as well as in this study too, we consider only the PMs of the sources, which is on the sky plane. In an HII region, where the ionizing star and the BRC both are not located at the sky plane, but have a significant distance along the line-of-sight, the  $|\theta_{ip} - \theta_{pm}| \sim 0^\circ$  might not always be satisfied because of the possible presence of a significant radial component of motion of the BRC/ionizing source. Apparently,  $180^\circ > |\theta_{ip} - \theta_{pm}| > 90^\circ$  might seem as a phenomenon opposite to RE in 2D, i.e. PMs of the YSOs towards the ionizing star, but these sources may have significant components of motions in the radial direction, which might make their total motions in 3D away from the ionizing star, satisfying the RE scenario. Thus, the  $|\theta_{ip} - \theta_{pm}| \sim 0^\circ$  condition does not signify the RE scenario completely in 2D, but in 3D.

A higher  $|\theta_{ip} - \theta_{pm}|$  for BRCs 54 and 89 signifies that the relative PM of the candidate YSOs direct towards their re-

spective ionizing sources. For BRC 54, we initially suspected that the presence of another massive star, HD 73882 (also considered to ionize BRC 55), might have influenced the motion of the candidate YSOs. But due to higher distance ( $\sim 13$  pc), the probability of HD 73882 influencing BRC 54 is low. Prisinzano et al. (2018) detected second generation of stars around BRC 54, which indicates that the kinematic coupling between the candidate YSOs and BRC 54 might have been lost. Therefore, the  $\theta_{pm}$  of the candidate YSOs might not indicate the PM of BRC 54.

The massive star considered to ionize BRC 89 is HD 165921, with respect to which  $\theta_{pm}$  of the candidate YSOs is estimated. Based on the 2MASS all-sky survey, Bica et al. (2003) discovered a stellar cluster encircling an ionizing source HD 166056, a B2Ve star (Herbst et al. 1982) in BRC 89. It is embedded in a cavity, surrounded by a prominent shell-like structure indicative of expanding ionization front (Santos et al. 2014). The pressure of HD 166056 might have affected the motion of the surrounding YSOs which is why  $\theta_{pm}$  of the candidate YSOs show significantly different direction in BRC 89.

#### 4 SUMMARY AND CONCLUSIONS

As an effect of the RDI mechanism, the compression of the BRCs because of ionization by the nearby OB stars results into triggered star formation. This leads to a group of young population staying behind the BRCs. Also, the BRCs escalate away from the direction of ionizing HII region as consequence of the photo-evaporation flow of cloud material in the direction of HII region, which is well-known as the Rocket Effect. Assuming that the internal projected motion of the YSOs imitates the same of their parental clouds in the sky plane, 22 BRCs (including BRC 18; Paper I) are investigated based on the astrometric measurements of the associated candidate YSOs obtained from the latest *Gaia* EDR3. As BRCs 54 and 89 show relatively higher  $|\theta_{ip} - \theta_{pm}|$ , we made two cases A and B, which indicates inclusion and exclusion of both the BRCs, respectively. The main outcomes of this work are summarized below:

- The Pearson's correlation coefficient of  $\theta_{ip}$  and  $\theta_{pm}$  for case A is found to be 0.909 with pnull  $4.641 \times 10^{-9}$ . For case B, the same is estimated as 0.967 with pnull  $3.444 \times 10^{-12}$ .
- The Spearman's correlation coefficient is found to be

0.899, with pnull as  $1.247 \times 10^{-8}$  for case A. For case B, the same is found to be 0.964 with pnull  $8.654 \times 10^{-12}$ .

- The statistic of K-S test is 0.182 with pvalue 0.821 and 0.200 with pvalue 0.771, for cases A and B, respectively.
- Based on the histogram of  $|\theta_{ip} - \theta_{pm}|$ , we found that most of the BRCs have a minimum of the difference between  $\theta_{ip}$  and  $\theta_{pm}$ .
- The strong correlation between  $\theta_{ip}$  and  $\theta_{pm}$  supports the RE in most of the BRCs on the plane-of-sky.

As the operating wavelength of *Gaia* is optical, the number of candidate YSOs detected is less possibly due to the presence of dense gas and dust surrounding them. More deep observations with good quality data would help us to increase the statistics and a better understanding.

## ACKNOWLEDGEMENTS

We are grateful to the referee, Dr. Alexander Slater Binks, for his careful examination and generous suggestions that considerably improved the quality of the manuscript. We acknowledge the support by the S. N. Bose National Centre for Basic Sciences under the Department of Science and Technology, Govt. of India. This work has made use of archival data from the European Space Agency (ESA) mission *Gaia* (<https://www.cosmos.esa.int/gaia>), processed by the *Gaia* Data Processing and Analysis Consortium (DPAC, <https://www.cosmos.esa.int/web/gaia/dpac/consortium>). Funding for the DPAC has been provided by national institutions, in particular the institutions participating in the *Gaia* Multilateral Agreement (MLA). DKO acknowledges the support of the Department of Atomic Energy, Government of India, under Project Identification No. RTI 4002.

## DATA AVAILABILITY

The *Gaia* EDR3 proper motions and distances of the sources are available in <https://vizier.u-strasbg.fr/viz-bin/VizieR-3?-source=I/350/gaiadr3> and <https://vizier.u-strasbg.fr/viz-bin/VizieR?-source=I/352>, respectively.

## REFERENCES

- Arun R., et al., 2021, *MNRAS*, **507**, 267  
 Bailer-Jones C. A. L., Rybizki J., Fouesneau M., Demleitner M., Andrae R., 2021, *AJ*, **161**, 147  
 Belokurov V., et al., 2020, *MNRAS*, **496**, 1922  
 Bertoldi F., 1989, *ApJ*, **346**, 735  
 Bertoldi F., McKee C. F., 1990, *ApJ*, **354**, 529  
 Bica E., Dutra C. M., Soares J., Barbuy B., 2003, *A&A*, **404**, 223  
 Buckner A. S. M., et al., 2020, *A&A*, **636**, A80  
 Chauhan N., Pandey A. K., Ogura K., Ojha D. K., Bhatt B. C., Ghosh S. K., Rawat P. S., 2009, *MNRAS*, **396**, 964  
 Choudhury R., Mookerjea B., Bhatt H. C., 2010, *ApJ*, **717**, 1067  
 Conti P. S., Leep E. M., 1974, *ApJ*, **193**, 113  
 Contreras M. E., Sicilia-Aguilar A., Muzerolle J., Calvet N., Berlind P., Hartmann L., 2002, *AJ*, **124**, 1585  
 Dale J. E., Haworth T. J., Bressert E., 2015, *MNRAS*, **450**, 1199  
 Elmegreen B. G., 1998, in Woodward C. E., Shull J. M., Thronson Jr. H. A., eds, Astronomical Society of the Pacific Conference Series Vol. 148, Origins. p. 150 ([arXiv:astro-ph/9712352](https://arxiv.org/abs/astro-ph/9712352))

- Gaia Collaboration Brown A. G. A., Vallenari A., Prusti T., de Bruijne J. H. J., Babusiaux C., Biermann M., 2020, arXiv e-prints, [p. arXiv:2012.01533](https://arxiv.org/abs/2012.01533)  
 Getman K. V., Feigelson E. D., Sicilia-Aguilar A., Broos P. S., Kuhn M. A., Garmire G. P., 2012, *MNRAS*, **426**, 2917  
 Getman K. V., Kuhn M. A., Feigelson E. D., Broos P. S., Bate M. R., Garmire G. P., 2018, *MNRAS*, **477**, 298  
 Hayashi M., Itoh Y., Oasa Y., 2012, *PASJ*, **64**, 96  
 Herbst W., Miller D. P., Warner J. W., Herzog A., 1982, *AJ*, **87**, 98  
 Hosoya K., Itoh Y., Oasa Y., Gupta R., Sen A. K., 2020, arXiv e-prints, [p. arXiv:2006.00219](https://arxiv.org/abs/2006.00219)  
 Ikeda H., et al., 2008, *AJ*, **135**, 2323  
 Ishida K., 1970, *PASJ*, **22**, 277  
 Kahn F. D., 1969, *Physica*, **41**, 172  
 Kervella P., Arenou F., Thévenin F., 2022, *A&A*, **657**, A7  
 Kounkel M., et al., 2018, *AJ*, **156**, 84  
 Kuhn M. A., Medina N., Getman K. V., Feigelson E. D., Gro-madzki M., Borissova J., Kurtev R., 2017, *AJ*, **154**, 87  
 Lindegren L., 2018, Re-normalising the astrometric chi-square in Gaia DR2, GAIA-C3-TN-LU-LL-124, [http://www.rssd.esa.int/doc\\_fetch.php?id=3757412](http://www.rssd.esa.int/doc_fetch.php?id=3757412)  
 Mercer E. P., Miller J. M., Calvet N., Hartmann L., Hernandez J., Sicilia-Aguilar A., Gutermuth R., 2009, *AJ*, **138**, 7  
 Morgan L. K., Thompson M. A., Urquhart J. S., White G. J., Miao J., 2004, *A&A*, **426**, 535  
 Ogura K., Sugitani K., Pickles A., 2002, *AJ*, **123**, 2597  
 Ogura K., Chauhan N., Pandey A. K., Bhatt B. C., Ojha D., Itoh Y., 2007, *PASJ*, **59**, 199  
 Oort J. H., 1954, Bull. Astron. Inst. Netherlands, **12**, 177  
 Oort J. H., Spitzer Jr. L., 1955, *ApJ*, **121**, 6  
 Panwar N., Chen W. P., Pandey A. K., Samal M. R., Ogura K., Ojha D. K., Jose J., Bhatt B. C., 2014, *MNRAS*, **443**, 1614  
 Panwar N., Pandey A. K., Samal M. R., Battinelli P., Ogura K., Ojha D. K., Chen W. P., Singh H. P., 2018, *AJ*, **155**, 44  
 Prisinzano L., Damiani F., Guarcello M. G., Micela G., Sciortino S., Tognelli E., Venuti L., 2018, *A&A*, **617**, A63  
 Saha P., Gopinathan M., Kamath U., Lee C. W., Puravankara M., Mathew B., Sharma E., 2020, *MNRAS*, **494**, 5851  
 Saha P., Maheswar G., Mathew B., Kamath U. S., 2021, *A&A*, **653**, A142  
 Saha P., Gopinathan M., Ojha D. K., Neha S., 2022, *MNRAS*, **510**, 2644  
 Santos F. P., Franco G. A. P., Roman-Lopes A., Reis W., Román-Zúñiga C. G., 2014, *ApJ*, **783**, 1  
 Sharma S., et al., 2016, *AJ*, **151**, 126  
 Sicilia-Aguilar A., Hartmann L. W., Hernández J., Briceño C., Calvet N., 2005, *AJ*, **130**, 188  
 Sicilia-Aguilar A., Patel N., Fang M., Roccatagliata V., Getman K., Goldsmith P., 2019, *A&A*, **622**, A118  
 Stassun K. G., Torres G., 2021, *ApJ*, **907**, L33  
 Sugitani K., Ogura K., 1994, *ApJS*, **92**, 163  
 Sugitani K., Fukui Y., Ogura K., 1991, *ApJS*, **77**, 59  
 Sugitani K., Tamura M., Ogura K., 1995, *ApJ*, **455**, L39  
 Thompson M. A., Urquhart J. S., White G. J., 2004, *A&A*, **415**, 627  
 Yamaguchi R., Saito H., Mizuno N., Mine Y., Mizuno A., Ogawa H., Fukui Y., 1999, *PASJ*, **51**, 791  
 Zari E., Hashemi H., Brown A. G. A., Jardine K., de Zeeuw P. T., 2018, *A&A*, **620**, A172  
 Zinnecker H., Yorke H. W., 2007, *ARA&A*, **45**, 481

This paper has been typeset from a *TEX/LAT<sub>E</sub>X* file prepared by the author.

**Table 1.** Kinematic properties of the candidate YSOs in the BRCs and the respective ionizing sources.

BRC Name*	HII region	Ionizing Star	$d$ (pc)	$\theta_{\text{pm}}(^{\circ})$	$\theta_{\text{ip}}(^{\circ})^{\dagger}$
(1)	(2)	(3)	(4)	(5)	(6)
SFO 2	Sh2-171	BD+66 1675	1027±69	14±16	8
SFO 5	IC 1805	BD+60 504	2007±236	340±14	291
SFO 7	IC 1805	BD+60 504	2192±31	2±4	31
SFO 11	IC 1848	HD 17505	2119±237	139±29	173
SFO 17	Sh2-264	$\lambda$ Ori	389±9	362±51	337
SFO 18 <sup>†</sup>	Sh2-264	$\lambda$ Ori	394±7	110±14	109
SFO 25	NGC 2264	HD 47839	692±12	25±21	3
SFO 26	Sh2-296	HD 54662	1236±127	229±3	224
SFO 27	Sh2-296	HD 53456	1095±71	374±31	314
SFO 31	Sh2-117	HD 199579	787±51	211±4	241
SFO 36	Sh2-131	HD 206267	902±47	250±101	276
SFO 37	Sh2-131	HD 206267	968±37	169±5	167
SFO 38	Sh2-131	HD 206267	923±41	11±7	16
SFO 39	Sh2-131	HD 206267	932±47	29±13	92
SFO 54	NGC 2626	vdBH17a	978±99	217±10	362
SFO 55	RCW 27	HD 73882	897±32	123±29	139
SFO 64	BBW 347	LSS2231	2968±225	28±20	37
SFO 65	RCW 62	HD 101205	2434±78	320±35	262
SFO 75	RCW 98	LSS 3423	1884±422	30±41	103
SFO 79	RCW 108	HD 150136	1515±263	304±21	246
SFO 82	RCW 113/116	HD 152233	1804±258	296±13	292
SFO 89	Sh2-29	HD 165921	1290±1394	233±7	124

\* BRCs are identified as SFO (Sugitani, Fukui, Ogura) in Simbad.

<sup>†</sup> Error in  $\theta_{\text{ip}}$  is negligible, hence not tabulated.

BRCs having  $\theta_{\text{ip}}$  and  $\theta_{\text{pm}} > 360^{\circ}$  are actually corrected for keeping minimum angular distance between these two. For example, BRC 17 has  $\theta_{\text{pm}} = 2^{\circ} \pm 51^{\circ}$ , but as  $\theta_{\text{ip}} = 337^{\circ}$ , we added  $360^{\circ}$  with  $\theta_{\text{pm}}$  to estimate the minimum  $|\theta_{\text{ip}} - \theta_{\text{pm}}|$ .

**Table 2.** Kinematic properties of the candidate YSOs in the BRCs and the respective ionizing sources.

candidate YSOs ( <i>Gaia</i> EDR3) (1)	RA (2)	Dec. (3)
SFO 2		
529108978383373824	0.817180	68.533421
529108913962819840	0.822722	68.528244
529116984202552064	0.891505	68.665579
529109562499260672	0.996169	68.546432
529109669877060096	0.999364	68.561558
529109704236796288	1.006998	68.570463
529110082193916416	1.007424	68.576971
529109704236795136	1.010965	68.573980
529110009175851648	1.019057	68.581070
529109631218432896	1.021873	68.564734
529109635517322240	1.023521	68.562283
529109631218428160	1.030511	68.561745
529109596858989184	1.031638	68.556941
529107981950942080	1.041955	68.514546
529109631218727680	1.048587	68.557023
529109596859011200	1.051103	68.546706
529109493779803392	1.058296	68.539329
529109394995715584	1.061381	68.546951
529109291919950080	1.062938	68.538589
529107226036641024	1.066895	68.457339
529107638353526912	1.086603	68.483371
529107638353525376	1.086814	68.481625
529106508781158656	1.280217	68.513387
SFO 5		
513565148141778560	37.017032	61.575681
513561716467377536	37.180873	61.526220
513560926193404544	37.181123	61.494877
513567209726131968	37.211332	61.665927
513562609820646656	37.256233	61.558057
513562919058291584	37.309085	61.557092
513586318040856064	37.423374	61.588046
SFO 7		
465931972268206208	38.472445	61.947325
465919808920854016	38.490779	61.887787
465918228372937600	38.558287	61.801810
465915062974574080	38.592096	61.757173
465915681452980736	38.633960	61.812643
465915612730624896	38.648419	61.810991
465914066542002688	38.673421	61.717098
465915406574942848	38.675025	61.782352
465922385902976640	38.765262	61.914548
SFO 11		
464554455998190592	42.856584	60.101325
464554421638442752	42.905852	60.107391
464555830388653568	42.965128	60.125149
464554284199714560	42.965341	60.112129
464555830387938048	42.967249	60.119478
464555830387929600	42.975882	60.128772
SFO 17		
3340887246596977664	82.375789	12.098617
3340893641804344320	82.469851	12.163148
3340894088480934400	82.490234	12.201947
3340894500797788672	82.502617	12.229013
3340882749767481344	82.515892	12.022681
3340892714091577856	82.554715	12.146044
3340896184424945664	82.570998	12.261384
3340888380468287488	82.608051	12.055951
3340889106319041024	82.650334	12.111273
3340890480708558848	82.715427	12.143540

**Table 2 – continued**

candidate YSOs ( <i>Gaia</i> EDR3) (1)	RA (2)	Dec. (3)
SFO 17		
3340878179922230272	82.754191	12.070638
3340878381785847296	82.754855	12.096842
3340878351720911872	82.783418	12.101767
3340878935836457472	82.802044	12.131820
334097311582846464	82.814597	12.189917
3340877935108760576	82.822064	12.096582
3340972806641584128	82.831061	12.154255
3340972733626479616	82.835537	12.154705
3340877728950818816	82.839460	12.095517
3340877728950193152	82.840267	12.096578
33408774224256986112	82.840446	12.043069
3340871028801247232	82.841301	11.915700
3340871067456399360	82.849493	11.927072
3340973558259384832	82.853259	12.202055
3340973631275296256	82.856891	12.214288
3340973352101788672	82.867039	12.197495
3340973596915556864	82.868331	12.209797
3340678446763632640	82.910861	11.807321
3340681981520082944	82.916445	11.847166
3340972497403927552	82.918674	12.179685
3340658415036209664	82.938609	11.631929
3340975551124339712	82.963700	12.272423
3341000736812880896	82.964315	12.554071
3340994556355913728	82.986524	12.419345
3340993869161153536	82.993690	12.379817
3340969061430118400	82.999760	12.135219
3341001256504863744	83.002221	12.570847
3340997064616797696	83.025877	12.473332
3340997133363271360	83.026715	12.489470
3340681088166923776	83.030248	11.901174
3340779838055977984	83.043450	12.050434
3340984072339594240	83.060387	12.408031
334096886063797248	83.064392	12.159503
3340984042275960832	83.081278	12.406744
3340774069916236800	83.109319	11.906737
3340774065621826048	83.111576	11.911601
3340984695110967296	83.143467	12.457907
3341008300251213824	83.169933	12.487643
3340984454592793088	83.179992	12.451460
3341007922294096896	83.189609	12.450624
3340764311750480384	83.266538	11.968315
3340761528611688960	83.287080	11.898705
SFO 18		
3336168314489240576	85.660435	9.310332
3336168043908536832	85.680581	9.287969
3336155189070384128	85.729819	9.246989
3336152375867856384	85.747103	9.164555
3336161549917961216	85.802402	9.283812
3336180585212965376	85.814037	9.491866
3336149519712868864	85.837176	9.101955
3336160690924950528	85.873411	9.283380
3336177454181082624	85.890385	9.496435
3336156121079561216	85.914989	9.178026
3336149867606924288	85.935460	9.133633
3336156292877976064	85.961132	9.206919
3336157422453353472	85.963992	9.227901
3336159419614147584	85.968111	9.283435
3336157873425925120	85.968650	9.266585
3336102897844570112	85.972911	9.119901
3336159557053093376	85.985790	9.304671
3336159282175185920	86.006802	9.289093
3336159071720837120	86.008674	9.260364

**Table 2 – continued**

candidate YSOs ( <i>Gaia</i> EDR3) (1)	RA (2)	Dec. (3)
SFO 18		
3336107772631258624	86.030253	9.110574
3336109048235617280	86.041829	9.144624
3336109563633776640	86.044381	9.212530
3336107429033839616	86.053240	9.086216
3336108223604259328	86.061986	9.135564
3336111006743055360	86.079400	9.209260
333610458147197440	86.080668	9.089784
3336158594980405248	86.080847	9.271995
3336158521965029888	86.087587	9.267106
3336108361043207168	86.090606	9.148215
3336108361043207168	86.091194	9.147915
3336109937294863872	86.095395	9.176425
3336110834944361984	86.107235	9.200320
3336105028148588032	86.108237	9.116840
3336109902935129088	86.112112	9.178385
3336104955132704768	86.119424	9.105122
3336256176637551104	86.137795	9.446547
3336110525706708992	86.154261	9.222194
3336104787630415872	86.157234	9.099283
3336256103621173248	86.158848	9.432716
3336107227171825664	86.194115	9.189299
3336204155993987072	86.220057	9.218111
3335326299037613056	86.226617	8.713875
3336093513339795456	86.267100	9.081243
SFO 25		
3326929118281227008	100.205037	9.960728
3326717466589159424	100.207263	9.882923
3326928705964373888	100.210787	9.915904
3326740728129988096	100.225458	9.873459
3326928847700236928	100.225790	9.931090
3326932004499068928	100.249125	10.036809
3326943897265235840	100.256368	10.248875
3326935960166062720	100.261885	10.119963
3326930874924790656	100.280257	9.975301
3326943927328338304	100.281154	10.251207
3326740521973590656	100.321865	9.908974
SFO 26		
3046018985610505600	105.931990	-11.615694
3046026540451631232	105.957919	-11.521443
3046025720119222784	105.974974	-11.546624
3046025715819957248	105.975102	-11.543665
3046025548320530304	105.991885	-11.544413
3046025440943675008	105.993075	-11.559610
3045831583295956224	106.005495	-11.604856
3045831617655703168	106.016364	-11.599203
3045830346345248384	106.022991	-11.664542
SFO 27		
3046026540451631104	105.957919	-11.521443
3046030427403041792	105.968721	-11.438005
3046026750911057408	105.970952	-11.493117
3046025715819957248	105.975102	-11.543665
3046027575540896256	105.984839	-11.428186
3046030564841979904	105.987988	-11.409098
3046027609900606976	106.005055	-11.425314
3046032072370037248	106.006838	-11.401754
3046027541185004544	106.009740	-11.427599
3046027335022717952	106.017002	-11.443177
304603217974968864	106.019563	-11.394363
3046029224812170240	106.024675	-11.399645
3046032656484579328	106.025013	-11.357863
3046032175450394624	106.025134	-11.387689

**Table 2 – continued**

candidate YSOs ( <i>Gaia</i> EDR3) (1)	RA (2)	Dec. (3)
SFO 27		
3046032214109395968	106.027125	-11.374434
3046032179749663232	106.027349	-11.387875
3046033829017076224	106.027389	-11.309653
3046028812495321088	106.027897	-11.435688
3046032901304147456	106.034603	-11.334795
3046033000084199424	106.038398	-11.321701
3046029259171897344	106.041477	-11.387892
30460408414583416832	106.051334	-11.299733
3046029667189515264	106.056360	-11.370099
3046028984293995520	106.057986	-11.411538
3046029568409539584	106.059362	-11.388029
3046026235515287552	106.064109	-11.478023
3046028915574513664	106.070001	-11.409016
3046029705848479744	106.083301	-11.372899
3046029396610840064	106.085899	-11.387360
3046027678624293888	106.094784	-11.464144
3046028571977483776	106.096879	-11.404809
3046028567676658688	106.107098	-11.403421
3045840688626813952	106.169933	-11.426916
3045840310669678080	106.187495	-11.466389
SFO 31		
2163139941968363520	312.655751	44.348055
2163139873248885632	312.668531	44.339344
2163140006394622208	312.677957	44.364693
2163139804527939968	312.702434	44.351252
2163139804529410944	312.702892	44.348122
2163140457364449920	312.723076	44.407410
2163140560443665152	312.723456	44.408447
2163140143827638272	312.724408	44.361061
2163136810933010048	312.728592	44.336789
2163140251206016640	312.728724	44.382835
2163136712151471360	312.734157	44.306060
2163140281266601728	312.744801	44.388165
2163136746512695424	312.745882	44.331735
2163136746511218176	312.747839	44.327502
2163137120170654720	312.758957	44.335850
2163140319925497088	312.763891	44.404285
2163136192456870016	312.831063	44.325146
SFO 36		
2178434217440720384	323.852133	57.550292
2178421813575206400	323.905550	57.478271
2178434389239575040	323.938735	57.557456
2178417656046880256	323.957301	57.401123
2178434561038259712	323.960316	57.596456
2178415834982840832	323.985635	57.347983
2178446002831454720	324.067038	57.580120
2178418167132388864	324.070784	57.444386
2178446342117152768	324.077924	57.607406
217844864649304576	324.093245	57.528092
2178445109478268416	324.098667	57.545841
2178418304571527680	324.104485	57.463934
217844899007898368	324.118437	57.537037
2178417278089774080	324.145473	57.436727
2178445624874345472	324.153753	57.568306
2178440741484235264	324.158434	57.449372
2178441604784967168	324.160031	57.488165
2178441909720014336	324.163107	57.498105
2178441914022611456	324.170965	57.502272
2178441707864184832	324.191461	57.492777
2178441742223922688	324.198437	57.498325
2178440470906711552	324.204093	57.421181
2178369930368001536	324.206879	57.374168

**Table 2 – continued**

candidate YSOs ( <i>Gaia</i> EDR3) (1)	RA (2)	Dec. (3)
SFO 36		
2178442115878750464	324.211327	57.519617
2178440913279379456	324.224007	57.478980
2178440814510995456	324.224779	57.466286
2178440642705389824	324.239399	57.458397
2178393398069567488	324.239518	57.389290
2178440642712309760	324.240275	57.459183
2178442081510495232	324.240962	57.518048
2178441291236505088	324.241322	57.486287
217844215450783104	324.247783	57.526332
2178393604228050432	324.253665	57.422881
2178442257613053952	324.254910	57.534543
2178442459476372480	324.255522	57.558474
2178441226827857920	324.256374	57.479491
2178440573992845568	324.260620	57.437321
2178441226827857920	324.262816	57.483628
2178440573992840448	324.263380	57.455095
2178447102343234048	324.265886	57.624686
2178393634282935040	324.274296	57.425248
2178442188900684032	324.275295	57.533776
2178440951949966848	324.279290	57.450210
2178442184589714944	324.282137	57.536404
2178444078686267648	324.283960	57.604479
2178441364259874304	324.284523	57.506525
2178393569868318208	324.287895	57.430134
2178441261187597056	324.289007	57.496765
2178441261187598336	324.289150	57.494766
2178441432986447360	324.293050	57.522256
2178441432986447872	324.293934	57.520104
2178394016544915456	324.294569	57.436194
2178441055029170688	324.297757	57.491271
2178443769448645376	324.298756	57.558096
2178394016544908288	324.300637	57.457276
2178443769448645632	324.301422	57.558842
2178394050904648448	324.307880	57.457498
2178440982007912704	324.311440	57.470808
2178441158101474560	324.312343	57.486782
2178441158108390144	324.312770	57.486519
2178394050904653312	324.316308	57.449764
2178393982185180160	324.318140	57.444534
217844113039290368	324.319114	57.605811
2178393947825444864	324.320866	57.438297
2178441085078071808	324.321454	57.479803
2178441089388915200	324.322358	57.489084
2178441089388913920	324.322583	57.490908
2178441192468289024	324.331546	57.513574
2178441089388920832	324.333159	57.479476
2178442876095464192	324.333704	57.526427
2178392229838569472	324.336028	57.350092
2178442669938739712	324.341791	57.512066
2178393982185185792	324.342839	57.445544
2178442876095465472	324.348673	57.531615
2178442974872913152	324.349750	57.548867
2178392917033317376	324.350403	57.403143
2178394188343600896	324.353173	57.485799
2178442704296780288	324.363834	57.524861
2178442699985787904	324.364255	57.523214
2178392848313851392	324.368435	57.390246
2178443941247336192	324.370589	57.601205
2178443013534417408	324.371514	57.548204
2178395661507500800	324.374572	57.487368
2178443112301672704	324.377703	57.583804
2178443116606937088	324.378112	57.574356
2178393054472271872	324.378334	57.416702

**Table 2 – continued**

candidate YSOs ( <i>Gaia</i> EDR3) (1)	RA (2)	Dec. (3)
SFO 36		
2178393054472273920	324.384810	57.417549
2178395597093125120	324.384830	57.490160
2178395592793859072	324.386841	57.474184
217844250484986880	324.389828	57.597511
2178442807375996160	324.390869	57.537961
2178442837424749056	324.398815	57.549550
217839452529441472	324.407814	57.479645
2178442738656256336	324.410436	57.527991
2178395631452868096	324.411854	57.493597
2178442841735735296	324.411907	57.547055
217844325844596224	324.418660	57.575885
2178443219692854528	324.420668	57.560143
2178395356574972928	324.420927	57.466933
2178450637088253696	324.424351	57.677820
2178443219692855040	324.424390	57.560675
2178443421539290880	324.425704	57.575414
2178443219693138688	324.428171	57.556967
2178443425852969728	324.428688	57.579511
2178395837611290112	324.435646	57.528416
2178392740924572672	324.437010	57.403748
2178389339310069760	324.438109	57.328373
2178395356574976256	324.438442	57.471469
2178443254045917696	324.442181	57.574461
2178395837599325696	324.445379	57.532251
2178394497581292800	324.446132	57.434589
2178395459654186240	324.452937	57.489681
21783897092029157120	324.453941	57.389113
2178396142543875840	324.455299	57.532880
2178443185333123584	324.459138	57.561200
217839556273396992	324.459288	57.502631
2178394291422867968	324.459296	57.430166
2178394699429915904	324.462830	57.463914
2178394531941272064	324.465701	57.447897
2178443284100355072	324.486562	57.580033
2178391302125646848	324.489868	57.405441
2178391199046443520	324.490090	57.379878
2178395975050256896	324.492197	57.522179
2178394669380222464	324.502463	57.473688
2178450538317241344	324.514567	57.693017
2178390958528283648	324.524777	57.378809
2178402262882609920	324.532163	57.598123
2178396009413394176	324.534021	57.524052
2178394394502336768	324.535220	57.446542
2178391370845370880	324.535333	57.419930
2178449232647211008	324.535644	57.618771
2178395081697083392	324.540760	57.495191
2178391130327213568	324.541678	57.397955
2178394768154306560	324.542438	57.452310
2178395253495768320	324.547566	57.517118
2178391370845370724	324.550076	57.416853
2178395287855504384	324.557715	57.528134
2178390305693267456	324.562898	57.365394
2178449816762756864	324.571359	57.657436
2178390305693509376	324.572937	57.375203
2178391881932722688	324.599781	57.460037
2178390649290896384	324.605400	57.386767
2178402056712608768	324.608188	57.569242
2178391989320655360	324.609953	57.477909
2178391680083024640	324.612183	57.444025
2178400888493119488	324.614296	57.518909
2178400888493120512	324.618131	57.518649
2178401232090491904	324.626306	57.548643
2178391611363553280	324.626488	57.438370

**Table 2 – continued**

candidate YSOs ( <i>Gaia</i> EDR3) (1)	RA (2)	Dec. (3)
SFO 36		
2178391607051821568	324.634026	57.443286
2178397864836157440	324.635643	57.504446
2178391611363558144	324.640927	57.434762
2178401025932067328	324.645041	57.547196
2178397899195898368	324.646700	57.503741
2178398002263548416	324.655419	57.517729
2178397830476432896	324.664847	57.487861
2178397521238551040	324.665652	57.464661
2178401640101582848	324.667773	57.573126
2178397516931971840	324.681268	57.457493
2178397551292322304	324.689294	57.473025
SFO 37		
2178110961019859200	325.111487	56.606547
2178110961019859328	325.113856	56.606019
2178110961019860864	325.119532	56.602676
SFO 38		
2178572790254904192	324.985110	58.229860
2178572515384121344	324.993569	58.204090
2178573198273201920	325.018974	58.253206
2178561309803684608	325.090679	58.245960
2178561309803669376	325.106798	58.241177
2178561245389942016	325.113851	58.239224
2178562791578166784	325.116659	58.253957
2178574744461539200	325.131643	58.298669
2178562516700266624	325.152326	58.229408
2178562551060090624	325.153795	58.243853
2178562752912981248	325.154343	58.250826
2178562447980793088	325.161832	58.217437
2178562482340616192	325.171263	58.233038
2178562654139305856	325.171512	58.253125
2178575156779164416	325.178405	58.327041
2178562649833718528	325.186884	58.250933
2178561412882638336	325.187700	58.187668
2178562654140703872	325.193728	58.256421
2178562684193256704	325.200132	58.260469
SFO 39		
2178252591856861440	326.315947	57.398345
2178253347771102336	326.392006	57.449805
2178253343467691904	326.403087	57.454570
2178302310399899136	326.460928	57.569224
2178254619081525248	326.475266	57.471767
2178249052803834240	326.501131	57.385957
2178254722160739328	326.506666	57.493876
2178255336331599104	326.567890	57.537926
2178254065020940544	326.608237	57.474642
SFO 54		
5528463903210289152	128.825305	-40.639072
5528463898908631296	128.827379	-40.638469
5528460982632433536	128.851861	-40.630607
5528462460101182336	128.857268	-40.625275
5528460913912957952	128.857845	-40.649441
5528460909612659840	128.858711	-40.647091
5528462391381705344	128.865797	-40.629472
5528460600376692224	128.878977	-40.683239
5528462215282558848	128.886545	-40.637564
5528459814401329152	128.900026	-40.685088
5528461326229815296	128.917863	-40.668665
5528461493728727808	128.919382	-40.643420

**Table 2 – continued**

candidate YSOs ( <i>Gaia</i> EDR3) (1)	RA (2)	Dec. (3)
SFO 55		
5525309679224303616	130.258108	-40.851611
5525309404343867008	130.272932	-40.879715
5525309404347345664	130.278144	-40.871491
5525315417300607744	130.297572	-40.834450
5525315348582080640	130.306144	-40.835407
5525314558307488384	130.312112	-40.864011
552531459266887040	130.319382	-40.858090
5525315451660343296	130.321984	-40.833414
5525314730105835904	130.342176	-40.840931
SFO 64		
5339406344853783168	168.040164	-58.777692
5339406344853784064	168.043617	-58.775652
5339406276134319872	168.083076	-58.768528
5339407792307371264	168.083896	-58.735824
5339406138695368448	168.090774	-58.789143
5339406276134323840	168.095506	-58.768474
5339385316693599232	167.970779	-58.830521
5339406173055110912	168.100420	-58.779458
5339407719243340544	168.111612	-58.750773
5339406211759383040	168.125793	-58.779075
SFO 65		
5333619447671205248	173.115031	-63.463595
5333606592810294656	173.268299	-63.514073
5333612537045149440	173.276352	-63.482744
SFO 75		
5884681167820754944	238.922042	-54.662066
588468127089841408	238.933403	-54.649745
5884681618820301184	238.974183	-54.635937
5884677972363578368	239.004325	-54.691620
SFO 79		
5940872985209320960	249.965948	-48.861551
5940872985201536640	249.973811	-48.862893
5940862986517159552	250.041070	-48.794521
5940860130322500992	250.065560	-48.913008
5940863192675559808	250.071388	-48.789952
5940862677279451648	250.079483	-48.836526
5940861783926211200	250.089274	-48.878902
5940860203378210816	250.095269	-48.908659
5940860199040422912	250.100495	-48.912007
5940861955724931328	250.112240	-48.839791
SFO 82		
5968283535216265088	251.786509	-41.270942
5968283397777300352	251.818542	-41.275009
5968283393435690752	251.828189	-41.269569
5968283874470676352	251.845438	-41.231744
5968271681105309312	251.850580	-41.272716
5968271990342949760	251.865275	-41.274959
SFO 89		
4066264896044933888	272.460228	-24.089038
4066264582463138048	272.463524	-24.097850
4066261528767982336	272.474727	-24.125813
4066264616822113536	272.482763	-24.102785
406626461666237504640	272.484526	-24.113703
4066264616822117248	272.485582	-24.108377
4066264621175030912	272.489631	-24.102080
4066261563127704064	272.490897	-24.121382
4066261661884621952	272.491424	-24.115998
4066261696237927808	272.501261	-24.108107